Dalton Transactions

An international journal of inorganic chemistry

Accepted Manuscript

This article can be cited before page numbers have been issued, to do this please use: C. J. Carrasco, F. Montilla, E. Alvarez González, A. Galindo, M. Pérez-Aranda, E. Pajuelo and A. Alcudia, *Dalton Trans.*, 2022, DOI: 10.1039/D1DT04213K.




ROYAL SOCIETY OF CHEMISTRY

rsc.li/dalton

View Article Online
DOI: 10.1039/D1DT04213K

ARTICLE

# Homochiral imidazolium-based dicarboxylate silver(I) compounds: synthesis, characterisation and antimicrobial properties.

Received 00th January 20xx,
Accepted 00th January 20xx

DOI: 10.1039/x0xx00000x

Carlos J. Carrasco,[a] Francisco Montilla,*[a] Eleuterio Álvarez,[b] Agustín Galindo,[a] María Pérez-Aranda,[c,d] Eloísa Pajuelo,[d] and Ana Alcudia*[c]

Complexes [Ag(L$^R$)], **2** (L$^R$ = 2,2'-(imidazolium-1,3-diyl)di(2-*alkyl*acetate)), were prepared by treatment of compounds HL$^R$, **1**, with $Ag_2O$. They were characterised by analytical, spectroscopic (IR, $^1$H and $^{13}$C NMR and polarimetry) and X-ray methods (**2c**, **2c'** and **2e**). In the solid state, these compounds are novel one-dimensional or two-dimensional coordination polymers in which silver(I) cations are connected via chiral [L$^R$]$^-$ anion with unprecedented coordination modes. The antimicrobial properties of these complexes were evaluated. **2a** and **2b'** showed the best antimicrobial properties (minimal inhibitory concentrations and minimal bactericidal concentration) for *Pseudomonas aeruginosa* and *Escherichia coli* pathogens. Eutomers **2b'** and **2c'** showed slightly better antimicrobial properties than their respective enantiomers **2b** and **2c**.

## Introduction

In the last decades, interest in chiral imidazolium-based dicarboxylate compounds has increased markedly.[1–3] They are synthesised easily from amino acids and are convenient starting precursors for the preparation of enantiopure substrates, such as ionic liquids[4] and *N*-heterocyclic carbene (NHC) ligands.[5–8] Additionally, they have been used as useful bridging ligands, acting as linkers, in the construction of homochiral coordination polymers or metal-organic frameworks,[9–11] and as chirality inductors in asymmetric catalysis.[12,13]

Recently we described the synthesis and characterization of chiral 2,2'-(imidazolium-1,3-diyl)bis(3-methylbutanoate) compounds of lithium, sodium and ammonium, {M[(*S*,*S*)-L$^{iPr}$]}$_n$ ($M^+$ = $Na^+$, $Li^+$ and $NH_4^+$), which included the first reported structural data for the chiral basic form [L$^R$]$^-$.[14] Following our interest in these ligands, we decided to investigate the analogous complexes of silver(I) and their antimicrobial properties. Due to the emerging problem of antibiotic resistance, looking for new compounds to inhibit the growth of bacterial pathogens has become indispensable.[15–20] The antimicrobial properties of silver complexes containing dicarboxylate,[21] amino acids,[22–25] chiral carboxylate[26–29] and *N*-heterocyclic carbene[30–38] coordinated ligands are well recognised, although precise action mechanisms have not yet been elucidated and are in research. Furthermore, these results suggest that antimicrobial properties depend on the nature of the ligand[37] and even a direct relationship between chirality and the antimicrobial effect has been observed.[39]

Here, we described the synthesis and characterization of new silver complexes **2**. Their antimicrobial properties were evaluated performing microbiological assays to determine minimal inhibitory concentrations (MIC) and minimal bactericidal concentration (MBC) as well as their mechanisms of action and their effect on biofilm formation, as a very important role in antimicrobial resistance development.[40]

## Results and discussion

### Synthesis and characterization of [Ag(L$^R$)] compounds

Complexes [Ag(L$^R$)], **2**, were prepared by reaction of compounds HL$^R$, **1**, with $Ag_2O$ in dried methanol and obtained as colourless or pale yellow crystals (Scheme 1). The 1:1 composition Ag:L$^R$ was confirmed by analytical data. HR-MS spectra showed fragmentation patterns that were consistent with the formation of [Ag(L$^R$)] species. The molecular ion displayed the appropriate isotopic ratio with the base peak at *m/z* 318.9850, 375.0474, 403.0787, 403.0787 and 403.0788 for complexes **2b-2f**, respectively. IR spectra of compounds **2** (Figs. S1-S6 at ESI) are characterised by a broad band in the 1620-1590 cm$^{-1}$ range, which was assigned to the antisymmetric COO vibrations of carboxylate groups. Additionally, symmetric COO vibrations appeared within the 1390-1370 cm$^{-1}$ range. NMR spectra ($^1$H and $^{13}$C{$^1$H}, Figs. S1- S6) show, in addition to the characteristic signals of the alkyl R group, a common pattern due to the imidazolium ring. Signals at *ca*. 7.5 and 122 ppm ($^1$H and $^{13}$C NMR, respectively) are due to the CH groups at the 4 and 5 positions, while signals at *ca*. 8.9 and 135 ppm ($^1$H and $^{13}$C NMR,

a. *Departamento de Química Inorgánica, Facultad de Química, Universidad de Sevilla, Aptdo 1203, 41071 Sevilla, Spain. E-mail: galindo@us.es.*
b. *Instituto de Investigaciones Químicas, CSIC-Universidad de Sevilla, Avda. Américo Vespucio 49, 41092 Sevilla, Spain.*
c. *Departamento de Química Orgánica y Farmacéutica, Universidad de Sevilla, 41012 Sevilla, Spain.*
d. *Departamento de Microbiología y Parasitología, Universidad de Sevilla, 41012 Sevilla, Spain.*

Electronic Supplementary Information (ESI) available: microbiological assays, crystal data, supramolecular packings, DFT profiles, optimised structures and their coordinates. See DOI: 10.1039/x0xx00000x

View Article Online
DOI: 10.1039/D1DT04213K



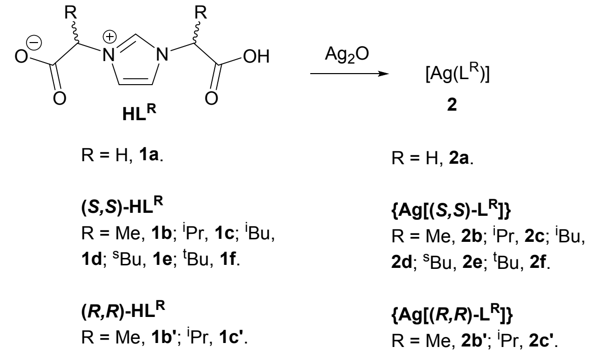


**Scheme 1** Synthesis of compounds **2**.

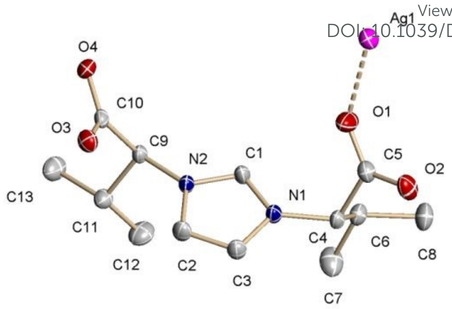


**Fig. 1** Asymmetric unit of compound {Ag[(*S*,*S*)-L$^{iPr}$]}$_n$ (**2c**), hydrogen atoms were omitted for clarity.

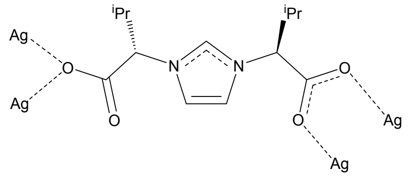


**Scheme 2** Coordination mode of [L$^{iPr}$]$^-$ anion in compound **2c**.

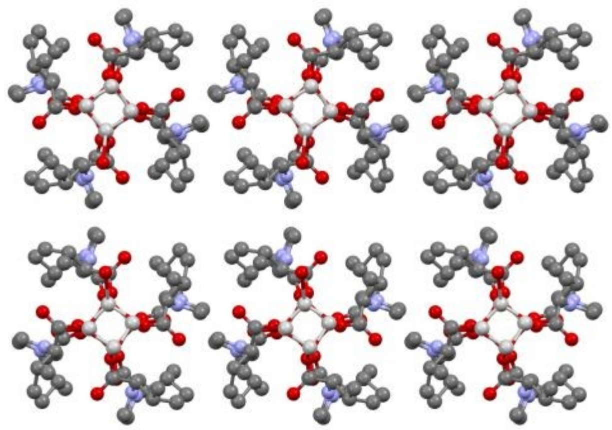

**Fig. 2** Comparison of the crystal packing in {Ag[(*S*,*S*)-L$^{iPr}$]}$_n$, **2c** (up), and {Ag[(*R*,*R*)-L$^{iPr}$]}$_n$, **2c'** (bottom), viewed along the *c* axis (three 1D coordination polymers). Hydrogen atoms omitted for clarity. Colour codes: C, dark grey; O, red; N, blue; Ag, light grey.

respectively) are assigned to the CH group of imidazolium at position 2. Additionally, carbon atoms of carboxylate groups resonate in the 172-176 ppm range. The specific chirality of the synthesized silver complexes was determined using polarimetry. Furthermore, the optical purity of the enantiomeric pairs **2b**-**2b'** and **2c**-**2c'** was also proven by electronic circular dichroism (CD) (Fig. S16).

### Structural characterization of compounds [Ag(L$^{iPr}$)], 2c and 2c', and [Ag(L$^{sBu}$)], 2e

Compounds **2c**, **2c'** and **2e** were analysed by single-crystal XRD methods. Selected bond distances and angles of these compounds are collected in Table S3 (ESI). Complex {Ag[(*S*,*S*)-L$^{iPr}$]}$_n$, **2c**, crystallises in the tetragonal system, $P4_1$ space group, and its asymmetric unit is constituted by the silver(I) and [L$^{iPr}$]$^-$ pair of ions (Fig. 1). The torsion angle C$_{carboxy}$-C$_{chiral}$-C'$_{chiral}$-C'$_{carboxy}$ of *ca*. 35° allows the simultaneous interaction of both carboxylate groups with up to four silver cations. The resulting coordination mode, $\mu_4$-$\kappa^2$O$^1$,$\kappa^1$O$^3$,$\kappa^1$O$^4$ (Scheme 2), is different from that reported for related sodium or ammonium compounds, {M[(*S*,*S*)-L$^{iPr}$]}$_n$ (M$^+$ = Na$^+$, NH$_4^+$),[14] and it is novel for this type of ligands. This specific bonding mode of [L$^{iPr}$]$^-$ anion arranges silver cations in an approximately linear disposition (Ag···Ag separations of 3.447(1) Å and a Ag···Ag···Ag angles of 138.4(1)° for **2c**, Fig. S7 at ESI) creating a polymeric one-dimensional (1D) chain. Compound {Ag[(*R*,*R*)-L$^{iPr}$]}$_n$, **2c'**, also crystallises in the tetragonal system, but in the $P4_3$ space group. Structural parameters (Table S3) and the overall geometry of **2c'** (Fig. S8) are obviously comparable to those of **2c**. In both compounds, the 1D polymer grows along *c* axis and follows a four-fold screw axis, within the $P4_1$ or $P4_3$ space groups. Therefore, the enantiomeric relationship between **2c** and **2c'** is clearly noticed when the 1D coordination polymer is viewed along this axis (Fig. 2). The supramolecular 3D arrangement in both complexes is attained by non-covalent interactions[41] between the hydrophobic parts ($^i$Pr groups) of the homochiral 1D-coordination polymers that afford a dense crystal packing (see Fig. S9). Compound {Ag[(*S*,*S*)-L$^{sBu}$]}$_n$, **2e**, crystallises in the monoclinic system, $P4_3$ space group, and again silver(I) and [L$^{sBu}$]$^-$ pair of ions appeared in its asymmetric unit (Fig. 3). The torsion angle C$_{carboxy}$-C$_{chiral}$-C'$_{chiral}$-C'$_{carboxy}$ of *ca*. 78° is higher than that observed in **2c**, but also permits the simultaneous coordination of both carboxylate groups with up to four silver cations. The coordination mode $\mu_4$-$\kappa^2$O$^1$, $\kappa^1$O$^2$,$\kappa^1$O$^3$,$\kappa^1$O$^4$ (Scheme 3) is also new for chiral imidazolium-dicarboxylate ligands. The subtle difference in the torsion angle, probably due to the different steric pressure of the alkyl R group, produces a growing of the coordination polymer in two dimensions. Fig. 4 shows the 2D coordination polymer viewed along *c* axis. Precisely, along this axis is encountered the nearly linear disposition of silver cations across the unit cell boundary with two distinct Ag···Ag separations of 3.956 and 4.047 Å and a Ag···Ag···Ag angle of 167.6°. For other structural parameters see Table S3.

### Solution behaviour of [Ag(L$^R$)] compounds

NMR spectra of **2** are similar to that reported for the parent compounds HL$^R$, **1**, with only small differences in chemical shifts, suggesting that the solid-state polymeric structure is not retained in solution. Additionally, $^1$H and $^{13}$C{$^1$H} NMR spectra

View Article Online
DOI: 10.1039/D1DT04213K



of compounds **2c** are almost identical to those of related M($L^{iPr}$) ($M^+$ = $Na^+$, $Li^+$, $NH_4^+$) compounds.[14] This fact suggests a total dissociation of the $M^+$ and $[L^R]^-$ ions in solution and a relatively minor influence of the cation type in the spectral pattern. To have a more precise information of this dissociation process, several conductivity measurements were carried out (see ESI). Compounds {Ag[(*S,S*)-$L^{iPr}$]}$_n$, **2c**, and {Na[(*S,S*)-$L^{iPr}$]}$_n$ show similar conductivities (around 80 μS/cm), but they are considerably lower than that determined for $AgNO_3$ or NaCl under the same experimental conditions (Table S1). Moreover, Diffusion Ordered NMR Spectroscopy (DOSY) experiments were done for precursor **1a**, silver complex {Ag[$L^H$]}$_n$, **2a**, and the sodium compound {Na[$L^H$]}$_n$ (Fig. S17). From these experiments, the diffusion coefficient of **2a** was calculated as $D = 5.5 \times 10^{-10}$ m$^2$/s, which was exactly the same than that observer for both precursor **1a** and compound {Na[$L^H$]}$_n$, respectively. These data agree with the rupture in solution of the polymeric nature of **2** and total dissociation of silver(I) cations occurred.

A variance in the $^1$H NMR spectra of **2** with respect to **1**, $HL^R$, is the reduced intensity of the resonance corresponding to the $C^2$-H group of imidazolium (at *ca*. 8.9 ppm). This suggests a fast H-D exchange with $D_2O$ at room temperature and was also reported by us in related M($L^{iPr}$) ($M^+$ = $Na^+$, $Li^+$, $NH_4^+$) compounds.[14] This observation was similarly noted in related imidazolium-dicarboxylate compounds and was explained on the basis of the acidity of this C-H moiety between the two N atoms.[42] However, when the $^1$H spectrum of $HL^{iPr}$ was recorded after one month in $D_2O$ solution at room temperature any indication of deuteration at this position was observed.[14] Therefore, the presence of the cation favours the H-D exchange, as similarly was evidenced for silver compounds **2**. A mechanism of the whole H-D exchange process was investigated by DFT methods for Na($L^{iPr}$) compound.[14] To compare the behaviour of the analogous silver(I) cation, DFT calculations were also carried out at the B3LYP/LANL2DZ/6-311++G** level for **2c**. Essentially, the proposed mechanism was the formation of a transient carbene intermediate that then is deuterated and has been discussed in detail for sodium cation.[14] For this reason, to avoid duplicity, most of the results are collected at ESI (profiles in Figs. S10-S12 and optimised structures) and here we highlight only major differences. Compounds (*S,S*)-$HL^{iPr}$ and **2c** and their isomeric carbene structures were optimised. While carbene of (*S,S*)-$HL^{iPr}$ lies 26.5 kcal·mol$^{-1}$ higher in energy than (*S,S*)-$HL^{iPr}$, by contrast carbene **2c** is stabilised by 3.0 kcal·mol$^{-1}$ (Fig. 5). The stabilization of these carbene intermediates come from the interaction of the silver(I) with the $C_{carbene}$ atom. The computed distance Ag-C = 2.202 Å is consistent with the values found in structurally characterised silver carbene complexes (from CSD search:[43] mean value for Ag-C of 2.12 Å). These results prompted us to study the possible isolation of this silver carbene species and these studies are now in progress.[44]

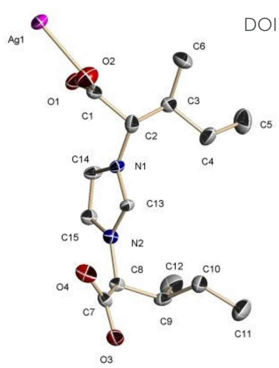


**Fig. 3** Asymmetric unit of compound {Ag[(*S,S*)-$L^{sBu}$]}$_n$ (**2e**), hydrogen atoms were omitted for clarity.

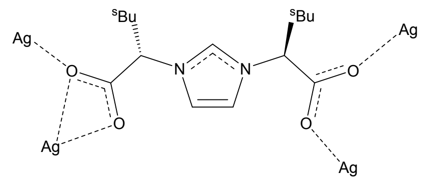


**Scheme 3** Coordination mode of $[L^{sBu}]^-$ anion in compound 2e.

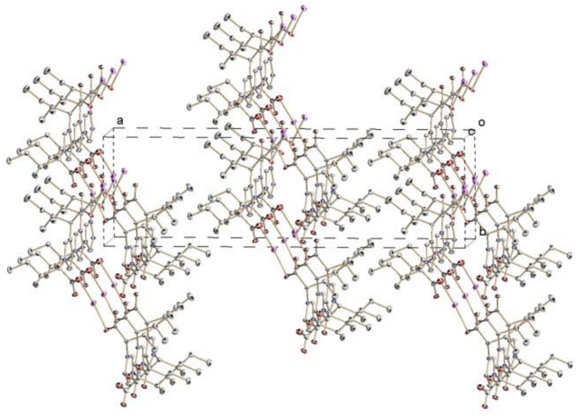


**Fig. 4** Crystal packing of three 2D coordination polymers of complex **2e**, viewed along *c* axis. Hydrogen atoms omitted for clarity.

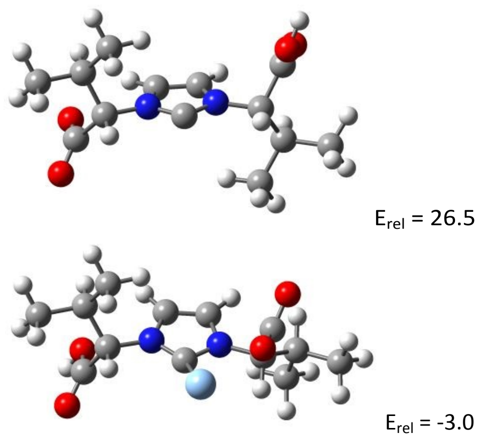


**Fig. 5** Optimised structure of carbene compounds, isomers of [(*S,S*)-$HL^{iPr}$] and **2c**, and their relative energies (kcal·mol$^{-1}$) with respect these compounds. Colour codes: C, grey; H, white; O, red; N, blue; Ag, light blue.

### Antimicrobial studies

#### Determination of minimal inhibitory growth concentrations (MIC) and minimal bactericidal concentrations (MBC)

Antimicrobial activities of compounds **2** were evaluated by MIC and MBC measurements. They did not show significant activity against Gram-positive strains *S. aureus* and *S. pseudintermedius* (not shown) and the study was focused on Gram-negative *E. coli* and *P. aeruginosa*. Results are shown in Table 1, where the MIC and MBC values for $AgNO_3$, a well-known antiseptic against Gram-negative bacteria,[45–47] are also included for an appropriate comparison under the same experimental conditions. Several MIC and MBC values of complexes **2** are lower than that of silver cation from $AgNO_3$ confirming that the activity is not only due to the dissociated $Ag^+$ ion, but a synergetic effect between the ionic pairs formed by the $Ag^+$ cation and the corresponding imidazolium-dicarboxilate anion, $[L^R]^-$. Interestingly, antimicrobial activities of ligand precursors **1** were also evaluated and they did not show activity towards Gram-negative (*E. coli* and *P. aeruginosa*) or Gram-positive strains (*S. pseudintermedius* and *S. aureus*).

**Table 1** Antimicrobial activities of complexes **2** and $AgNO_3$ evaluated by MIC and MBC ($mg{\cdot}L^{-1}$).

| | E. coli | | P. aeruginosa | |
|---|---|---|---|---|
| **Complex** | **MIC** | **MBC** | **MIC** | **MBC** |
| **2a** | 16 | 64 | 8 | 32 |
| **2b** | 32 | 128 | 16 | 128 |
| **2b’** | 32 | 64 | 4 | 32 |
| **2b-rac** | 32 | 64 | 4 | 32 |
| **2c** | 64 | 128 | 32 | 64 |
| **2c’** | 32 | 128 | 16 | 32 |
| **2c-rac** | 32 | 128 | 16 | 32 |
| **2d** | 64 | 256 | 32 | 256 |
| **2e** | 32 | 256 | 64 | 128 |
| **2f** | 64 | 512 | 16 | 256 |
| **$AgNO_3$** | 16 | 32 | 8 | 16 |

**2a** showed the best MIC and MBC values of all silver complexes. In particular, MIC concentrations are comparable in both *E. coli* and *P. aeruginosa* pathogens than those obtained for $AgNO_3$, while a slightly higher MBC value was observed for *E. coli*. In *P. aeruginosa* assays. **2b’** has comparable antimicrobial activity as **2a**. Therefore, for *E. coli,* complex **2a** is the most effective antimicrobial agent, while for *P. aeruginosa* both **2a** and **2b’** show the best antimicrobial properties. Interestingly, these results evidence slight differences in antimicrobial activity between enantiomeric pairs of complexes **2b** and **2b’** and **2c** and **2c’**, which could be related to the mechanism of action of these compounds. The eutomers for both bacteria are complexes **2b’** and **2c’**, which were prepared with the precursor ligands **1b’** and **1c’** from the non-proteinaceous amino acids *D*-alanine and *D*-valine, respectively. Comparable results were obtained in the antimicrobial study of amino acid-based ionic liquids and poly(ionic liquid) membranes in which those based on *D*-enantiomeric amino acid showed higher antibacterial activities compared to those of the corresponding *L*-enantiomers.[39] From all **2** compounds, **2a** demonstrates to be an effective antimicrobial agent for both bacteria and could be considered a possible alternative to classical drugs.

#### Determination of antioxidant enzymes and thiobarbituric acid reactive substances (TBARs)

The determination of antioxidant enzymes and thiobarbituric acid reactive substances (TBARs) of complex **2c**´ towards both *E. coli* and *P. aeruginosa*, as well as its stereoisomer **2c**, was performed to elucidate the antimicrobial mechanism. Results are presented in Table 2 and they show that the detoxification mechanisms against oxidative stress (ROS) manifested in both *E. coli* and *P. aeruginosa* are different. While in *E. coli* this detoxification is mediated by catalase enzyme, in *P. aeruginosa* is mainly mediated by Superoxide dismutase, which evidences strong activity of 6 to 20-fold the control. The malondialdehyde (MDA) quantification, one of thiobarbituric acid reactive substances (TBARs), considered as an indication of membrane damage due to ROS,[48] showed that for complex **2c**, MDA levels both at MIC and MBC were lower than the control in both *E. coli* and *P. aeruginosa* assays (Fig. S13). By contrast, MDA levels for complex **2c**´ were higher than control at MBC in both *E. coli* and at MIC in *P. aeruginosa* assays (Fig. S14).

#### Effects on biofilm formation: evaluation by colorimetric technique and by Scanning Electron Microscopy (SEM)

Due to the different antimicrobial activity of complex **2c’**, towards both *E. coli* and *P. aeruginosa*, with respect to its stereoisomer **2c**, the determination of the effect of these complexes on biofilm formation, a very important virulence factor in bacteria, was evaluated by two different techniques: colorimetric method[49] and SEM. Experiments showed that both complexes **2c** and **2c’** were capable of inhibit biofilm formation at lower concentrations than MIC in *E. coli* assays. However, in *P. aeruginosa* biofilm formation was affected when MIC was reached (Table 3).

**Table 2** Antioxidant enzyme activity ($mU{\cdot}mg^{-1}$ protein) of complexes **2c** and **2c**´ in *E. coli* and *P. aeruginosa* assays.[a]

| | | *E. coli* | | | *P. aeruginosa* | | |
|---|---|---|---|---|---|---|---|
| **Complex** | **Enzyme** | **Control** | **MIC** | **MBC** | **Control** | **MIC** | **MBC** |
| **2c** | Catalase | ND[b] | $1.2 \times 10^{-5} \pm 0.1 \times 10^{-5}$ | $5.7 \times 10^{-5} \pm 0.7 \times 10^{-5}$ | ND | ND | ND |
| **2c**´ | Catalase | ND | ND | $6.0 \times 10^{-5} \pm 0.9 \times 10^{-5}$ | ND | ND | ND |
| **2c** | Peroxidases | 0.49 ± 0.05 | 1.1 ± 0.2 | 0.88 ± 0.02 | 0.38 ± 0.03 | 0.9± 0.1 | 2.3 ± 0.3 |
| **2c**´ | Peroxidases | 0.49 ± 0.05 | 1.0 ± 0.1 | 1.3 ± 0.2 | 0.38 ± 0.03 | 1.0 ± 0.1 | 0.66± 0.06 |
| **2c** | Superoxide dismutase | 3.33 ± 0.01 | 2.60 ± 0.01 | 3.44 ± 0.01 | 3.40 ± 0.06 | 9. 6 ± 0.2 | 22.3 ± 0.3 |
| **2c**´ | Superoxide dismutase | 3.33 ± 0.01 | 2.46 ± 0.01 | 3.06 ± 0.01 | 3.40 ± 0.06 | 2.98 ± 0.03 | 3.47± 0.05 |

[a] Data are means ± standard deviations of three independent determinations. [b] ND = not detected.

View Article Online
DOI: 10.1039/D1DT04213K







**Table 3** Determination of the onset inhibitory concentration ($mg{\cdot}L^{-1}$) of biofilm formation for complexes **2c** and **2c´** in comparison to MIC ($mg{\cdot}L^{-1}$).

| | *E. coli* | | *P. aeruginosa* | |
|---|---|---|---|---|
| Complex | MIC | Onset inhibitory concentration of biofilm | MIC | Onset inhibitory concentration of biofilm |
| **2c** | 64 | 32 | 64 | 64 |
| **2c´** | 32 | 16 | 32 | 32 |

The formation of biofilms onto a glass surface was additionally evaluated by SEM. As can be observed in Fig. 6 for **2c’** and Fig. S15 for **2c**, both complexes were very effective in inhibiting bacterial growth and biofilm formation. Moreover, deformation and damage to the bacterial walls were clearly appreciated at MIC and MBC values.

## Experimental

All synthetic preparations were carried out under nitrogen atmosphere, while other operations were carried out under aerobic conditions. Solvents were purified and dried appropriately prior to use, using standard procedures. Chemicals were obtained from commercial sources and used as supplied. Compounds $HL^R$ were prepared according to the literature procedures.[1,13] Infrared spectra were recorded on Perkin-Elmer FT-IR Spectrum Two spectrophotometer, in pressed KBr pellets or using the ATR technique. NMR spectra were recorded on Bruker AMX-300 or Avance III spectrometers at the *Centro de Investigaciones, Tecnología e Innovación* (CITIUS) of the University of Sevilla by using Avance III spectrometers with $^1$H and $^{13}$C{$^1$H} NMR shifts referenced to the residual signals of deuterated solvents. All data are reported in ppm downfield from $Si(CH_3)_4$. Polarimetry was carried out using a JASCO P-2000 Digital Polarimeter and the measurements were made at room temperature (concentration of *ca*. 1-3 mg/mL). Conductivities of freshly prepared $1.0{\cdot}10^{-3}$ M water solutions at *ca*. 25 °C were measured for the substrates using a Crison Basic 30 conductivity meter, calibrated with KCl Crison standard solutions of concentrations 147 µS/cm, 1413 µS/cm and 12.88 mS/cm, respectively. Elemental analyses (C, H, N) and high-resolution mass spectra were conducted by the CITIUS of the University of Sevilla on an Elemental LECO CHNS 93 analyser and on a QExactive Hybrid Quadrupole-Orbitrap Mass Spectrometer from Thermo Scientific, respectively.

**Syntheses of silver compounds.** The following synthetic procedure is general and specific details appear for each complex. Over a solution of $HL^R$ (1.00 mmol) in dried MeOH (8-10 mL) $Ag_2O$ (0.116 g, 0.50 mmol) was added. The mixture was stirred for 16h at room temperature in the dark. Then, the mixture was filtered and the resulting solid was dissolved in water. Slow evaporation of this solution at room temperature, in a dark box to avoid photolysis decomposition, resulted in the formation of colourless or pale-yellow crystals of the silver compound.

**Silver 2,2'-(imidazolium-1,3-diyl)diacetate, $[Ag(L^H)]_n$ (2a).** Colorless crystals of **2a**. Yield: 0.220 g, 76 %. IR ($cm^{-1}$): 3142 (w), 3098 (m), 3056 (m), 2986 (w), 1603 (vs), 1586 (vs), 1562 (s), 1427 (w), 1386 (vs), 1346 (s), 1307 (s), 1286 (s), 1214 (s), 1196 (w), 1172 (s), 1107 (w), 1030 (w), 967 (w), 921 (m), 876 (m), 788 (m), 768 (s), 701 (m), 684 (vs), 627 (s), 576 (s), 448 (m). $^1$H NMR ($D_2O$, 300 Hz): δ 4.83 (s, 4H, C$H_2$), 7.44 (s, 2H, C*H*, $H^4/H^5$), 8.74 (s, 1H, C*H*, $H^2$). $^{13}$C{$^1$H} NMR ($D_2O$, 75.47 Hz): δ 52.0 (s, $CH_2$), 123.2 (s, *C*H, $C^4/C^5$), 137.2 (s, *C*H, $C^2$), 172.3 (s, *C*OO). Elemental Anal. Calc. for $C_7H_7N_2O_4Ag$: C, 28.89; H, 2.42; N, 9.63. Found: C, 29.34; H, 2.66; N, 9.73 %.

**Silver 2,2'-(imidazolium-1,3-diyl)dipropionate, $[Ag(L^{Me})]_n$ (2b and 2b’).** Colourless crystals of {Ag[(*S,S*)-$L^{Me}$]}$_n$ (**2b**). Yield: 0.160 g, 47 %. IR ($cm^{-1}$): 3089 (w), 3016 (w), 1642 (m), 1593 (vs), 1548 (s), 1456 (m), 1413 (m), 1382 (s), 1358 (s), 1334 (s), 1259 (s), 1166 (s), 1122 (w), 1085 (w), 1073 (w), 1036 (w), 972 (w), 909 (w), 877 (m), 817 (w), 782 (m), 742 (w), 705 (w), 686 (s), 655 (m), 579 (w), 526 (w), 481 (w), 443 (m). $^1$H NMR ($D_2O$, 300 Hz): δ 1.76 (d, $^3J_{HH}$ = 7.4 Hz, 6H, CHC$H_3$), 4.99 (c, $^3J_{HH}$ = 7.4 Hz, 2H, C*H*CH$_3$), 7.51 (s, 2H, C*H*, $H^4/H^5$), 8.85 (s, 1H, C*H*, $H^2$). The latter signal is partially deuterated. $^{13}$C{$^1$H} NMR ($D_2O$, 75.47 Hz): δ 17.6 (s, CH*C*H$_3$), 60.3 (s, *C*HCH$_3$), 121.5 (s, *C*H, $C^4/C^5$), 134.8 (s, *C*H, $C^2$), 175.5 (s, *C*OO). $[\alpha]_D^{25}$ = +37.4° ± 1.3° ($H_2O$). HR-MS (negative mode), found: m/z = 318.9850, calculated for $C_9H_{12}N_2O_4Ag^+$, 318.9843. Elemental Anal. Calc. for $C_9H_{13}N_2O_5Ag$ (**2b**·$H_2O$): C, 32.07; H, 3.89; N, 8.31. Found: C, 32.14; H, 3.88; N, 8.29 %. Colourless crystals of {Ag[(*R,R*)-$L^{Me}$]}$_n$ (**2b’**). Yield: 0.180 g, 48 %. IR and $^1$H and $^{13}$C{$^1$H} NMR spectra were identical to those of its enantiomer **2b**. $[\alpha]_D^{25}$ = -30.7° ± 0.6° ($H_2O$). HR-MS (negative mode), found: m/z = 318.9850, calculated for $C_9H_{12}N_2O_4Ag^+$, 318.9843. Elemental Anal. Calc. for $C_9H_{13}N_2O_5Ag$ (**2b’**·$H_2O$): C, 32.07; H, 3.89; N, 8.31. Found: C, 31.89; H, 3.61; N, 8.25 %.

**Silver 2,2'-(imidazolium-1,3-diyl)bis(3-methylbutanoate), $[Ag(L^{iPr})]_n$ (2c and 2c’).** Colourless crystals of compound {Ag[(*S,S*)-$L^{iPr}$]}$_n$ (**2c**). Yield: 0.160 g, 43 %. IR ($cm^{-1}$): 3127 (m), 3080 (m), 2964 (m), 1620 (vs), 1595 (vs), 1546 (s), 1471 (m), 1462 (m), 1371 (vs), 1352 (s), 1260 (s), 1238 (s), 1159 (s), 1123 (w), 1105 (w), 1028 (w), 959 (w), 933 (w), 919 (w), 844 (w), 813 (m), 776 (s), 748 (s), 723 (s), 704(m), 636 (m), 475 (w), 449 (w). $^1$H NMR ($D_2O$, 300 Hz): δ 0.78 (d, $^3J_{HH}$ = 7 Hz, 6H, CHC$H_3$), 0.89 (d, $^3J_{HH}$ = 7 Hz, 6H, CHC$H_3$), 2.39 (o, $^3J_{HH}$ = 7 Hz, 2H, C*H*CH$_3$), 4.52

View Article Online
DOI: 10.1039/D1DT04213K





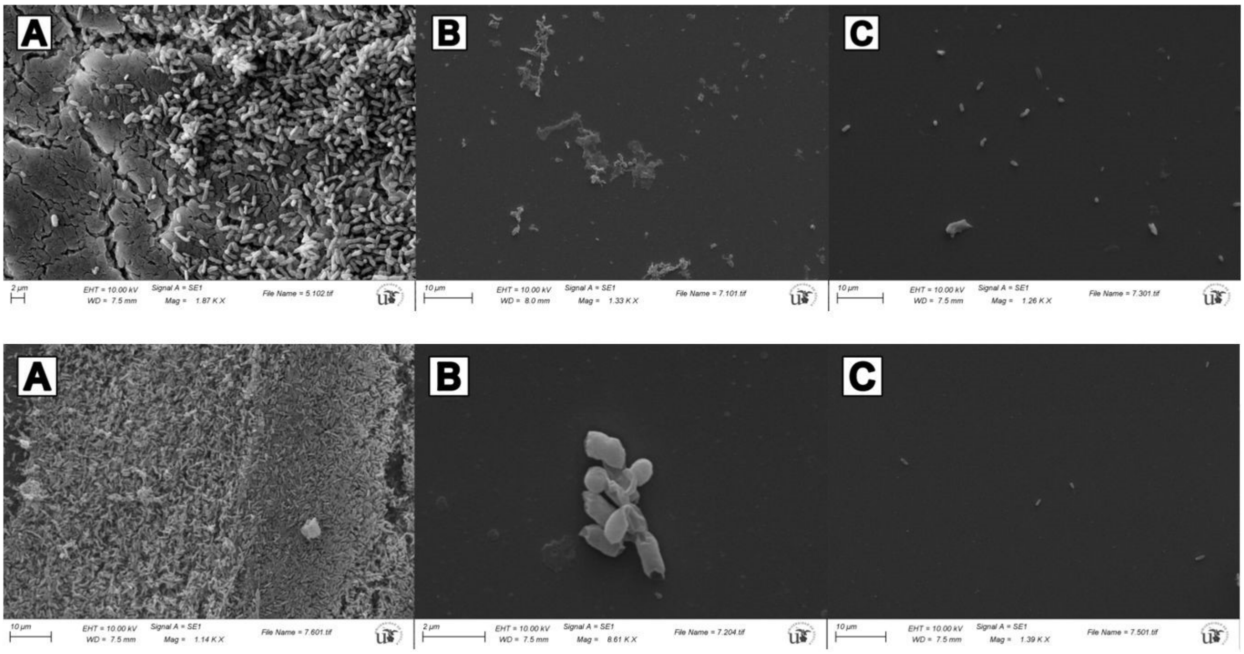


**Fig. 6** Evaluation of biofilm formation of *E. coli* (top) and *P. aeruginosa* (bottom) exposed to complex **2c'** (A: control, B: MIC, C: MBC).

(d, $^3J_{HH}$ = 7.8 Hz, 2H, C*H*CH(CH$_3$)$_2$, 7.51 (s, 2H, C*H*, H$^4$/H$^5$), 8.89 (s, 1H, C*H*, H$^2$). The latter signal is partially deuterated. $^{13}$C{$^1$H} NMR (D$_2$O, 75.47 Hz): δ 17.5 (s, CH*C*H$_3$), 18.6 (s, CH*C*H$_3$), 31.1 (s, *C*HCH$_3$), 71.5 (s, *C*HCH(CH$_3$)$_2$), 121.9 (s, *C*H, C$^4$/C$^5$), 135.7 (s, *C*H, C$^2$), 173.8 (s, *C*OO). [α]$_D$$^{25}$ = +84.9° ± 0.7° (H$_2$O). HR-MS (negative mode), found: m/z = 375,0474, calculated for $C_{13}H_{20}N_2O_4Ag^+$, 375.0469. Elemental Anal. Calc. for $C_{13}H_{19}N_2O_4Ag$: C, 41.62; H, 5.10; N, 7.47. Found: C, 41.30; H, 5.02; N, 7.51 %. Colourless crystals of compound {Ag[(*R,R*)-L$^{iPr}$]}$_n$ (**2c'**). Yield: 0.112 g, 30 %. IR and $^1$H and $^{13}$C{$^1$H} NMR spectra were identical to its enantiomer 2c'. [α]$_D$$^{25}$ = -87.0° ± 0.3° (H$_2$O). HR-MS (negative mode), found: m/z = 375.0474, calculated for $C_{13}H_{20}N_2O_4Ag^+$, 375.0469. Elemental Anal. Calc. for $C_{13}H_{19}N_2O_4Ag$: C, 41.62; H, 5.10; N, 7.47. Found: C, 41.14; H, 5.05; N, 7.46 %.

**Silver 2,2'-(imidazolium-1,3-diyl)bis(4-methylpentanoate), {Ag[(*S,S*)-L$^{iBu}$]}$_n$ (2d).** In this case, the reaction mixture was centrifugated under N$_2$ atmosphere, filtered and the filtrate was concentrated to dryness obtaining a yellow-brownish microcrystalline solid of 2d. Yield: 0.246 g, 61 %. IR (cm$^{-1}$): 3134 (w), 3095 (w), 2966 (m), 2956 (m), 2870 (m), 1594 (vs), 1467 (m), 1366 (vs), 1281 (m), 1238 (w), 1163 (s), 1123 (m), 1047 (w), 1009 (w), 962 (w), 922 (w), 895 (w), 838 (w), 736 (s), 695 (s), 641 (m), 537 (w), 498 (m), 442 (w), 427 (w), 419 (w). $^1$H NMR (D$_2$O, 500 Hz): δ 0.83 (t, $^3J_{HH}$ = 7.0 Hz, 12H, CH$_2$CH(C*H*$_3$)$_2$), 1,26 (m, $^3J_{HH}$ = 7.0 Hz, 2H, CH$_2$C*H*(CH$_3$)$_2$), 1.96 (m, $^3J_{HH}$ = 7.0 Hz, 4H, C*H*$_2$CH(CH$_3$)$_2$), 4.86 (dd, $^3J_{HH}$ = 10.9 Hz, 2H, C*H*$^i$*Bu*), 7.50 (s, 2H, C*H*, H$^4$/H$^5$), 8.92 (s, 1H, C*H*, H$^2$). $^{13}$C{$^1$H} NMR (D$_2$O, 125,78 Hz): δ 20.2 (s, CH$_2$CH(*C*H$_3$)$_2$), 22.0 (s, CH$_2$CH(*C*H$_3$)$_2$), 24.5 (s, CH$_2$*C*H(CH$_3$)$_2$), 40.6 (s, *C*H$_2$CH(CH$_3$)$_2$), 63.6 (s, *C*H$^i$Bu), 121.7 (s, *C*H, C$^4$/C$^5$), 135.4 (s, *C*H, C$^2$), 175.0 (s, *C*OO). [α]$_D$$^{25}$ = +39.2° ± 0.1° (H$_2$O). HR-MS (negative mode), found: m/z = 403.0787, calculated for $C_{15}H_{24}N_2O_4Ag$, 403.0782. Elemental Anal. Calc. for $C_{15}H_{25}N_2O_5Ag$ (2d·H$_2$O): C, 42.77; H, 5.98; N, 6.65. Found: C, 42.89; H, 5.73; N, 6.69 %.

**Silver 2,2'-(imidazolium-1,3-diyl)bis(3-methylpentanoate), {Ag[(*S,S*)-L$^{sec\text{-}Bu}$]}$_n$ (2e).** Colourless crystals of **2e**. Yield: 0.259 g, 64 %. IR (cm$^{-1}$): 3424 (w), 3130 (w), 2966 (m), 2928 (w), 2873 (w), 1591 (vs), 1564 (m), 1544 (m), 1461 (w), 1454 (w), 1421 (w), 1379 (vs), 1329 (w), 1306 (w), 1253 (w), 1221 (w), 1177 (w), 1159 (m), 1125 (w), 1093 (w), 1033 (w), 1019 (w), 980 (w), 959 (w), 926 (w), 908 (w), 844 (w), 813 (m), 776 (s), 742 (s), 653 (w), 570 (w), 520 (w), 415 (w). $^1$H NMR (D$_2$O, 500 Hz): δ 0.82 (t, $^3J_{HH}$ = 7.0 Hz, 6H, CH$_3$CHCH$_2$C*H*$_3$), 0.92 (d, $^3J_{HH}$ = 7.0 Hz, 6H, C*H*$_3$CHCH$_2$CH$_3$), 1,01 (m, $^3J_{HH}$ = 7.0 Hz, 2H, CH$_3$CHC*H*$_2$CH$_3$), 1,27 (m, $^3J_{HH}$ = 7.0 Hz, 2H, CH$_3$CHC*H*$_2$CH$_3$), 2.19 (m, $^3J_{HH}$ = 7.0 Hz, 2H, CH$_3$C*H*CH$_2$CH$_3$), 4.60 (d, $^3J_{HH}$ = 8,1 Hz, 2H, C*Hsec-Bu*), 7.54 (s, 2H, C*H*, H$^4$/H$^5$), 8.91 (s, 1H, C*H*, H$^2$). $^{13}$C{$^1$H} NMR (D$_2$O, 125,78 Hz): δ 10.3 (s, CH$_3$CHCH$_2$*C*H$_3$), 15.1 (s, *C*H$_3$CHCH$_2$CH$_3$), 24.6 (s, CH$_3$CH*C*H$_2$CH$_3$), 37.3 (s, CH$_3$*C*HCH$_2$CH$_3$), 70.6 (s, *C*Hsec-Bu), 122.0

(s, *C*H, $C^4/C^5$), 135.7 (s, *C*H, $C^2$), 173.9 (s, *C*OO). $[\alpha]_D^{25}$ = +30.4° ± 0.2° ($H_2O$). HR-MS (negative mode), found: m/z = 403.0787, calculated for $C_{15}H_{24}N_2O_4Ag$, 403.0782. Elemental Anal. Calc. for $C_{15}H_{27}N_2O_6Ag$ (**2e**·$2H_2O$): C, 41.02; H, 6.20; N, 6.38. Found: C, 41.05; H, 5.96; N, 6.39 %.

**Silver 2,2'-(imidazolium-1,3-diyl)bis(3,3-dimethylbutanoate), {Ag[(*S,S*)-L$^{t\text{-}Bu}$]}$_n$ (2f).** In this case, the reaction mixture was centrifuged under $N_2$ atmosphere, filtered and the filtrate was concentrated to dryness obtaining a yellow microcrystalline solid of **2f**. Yield: 0.236 g, 59 %. IR ($cm^{-1}$): 3737 (w), 3134 (w), 3082 (w), 2958 (w), 2912 (w), 2873 (w), 1604 (vs), 1579 (s), 1558 (m), 1539 (m), 1479 (m), 1401 (w), 1367 (s), 1260 (m), 1229 (m), 1211 (m), 1181 (m), 1147 (m), 1104 (m), 1034 (m), 961 (w), 934 (w), 824 (w), 746 (s), 701 (w), 652 (m), 491 (w), 457 (w), 440 (w), 432 (w), 414 (w). $^1$H NMR ($D_2O$, 500 Hz): δ 0.74 (s, 18H, C(C*H*$_3$)$_3$), 4.48 (s, 2H, C*H*$^t$Bu), 7.35 (s, 2H, C*H*, $H^4/H^5$), 8.94 (s, 1H, C*H*, $H^2$). $^{13}$C{$^1$H} NMR ($D_2O$, 125,78 Hz): δ 26.4 (s, C(*C*H$_3$)$_3$), 34.3 (s, *C*(CH$_3$)$_3$), 74.2 (s, *C*H$^t$Bu), 122.3 (s, *C*H, $C^4/C^5$), 136.4 (s, *C*H, $C^2$), 172.7 (s, *C*OO). $[\alpha]_D^{25}$ = +109.1° ± 0.1° ($H_2O$). HR-MS (negative mode), found: m/z = 403.0788, calculated for $C_{15}H_{24}N_2O_4Ag$, 403.0782. Elemental Anal. Calc. for $C_{15}H_{25}N_2O_5Ag$ (**2f**·$H_2O$): C, 42.77; H, 5.98; N, 6.65. Found: C, 43.03; H, 5.98; N, 6.70 %.

**Single-Crystal X-ray Crystallography.** A summary of the crystallographic data and structure refinement results for compounds **2c**, **2c'** and **2e** is given in Table S2 (ESI). Crystals of suitable size for X-ray diffraction analysis were coated with dry perfluoropolyether and mounted on glass fibres and fixed in a cold nitrogen stream (T = 213 K) to the goniometer head. Data collection was performed on a Bruker-Nonius X8Apex-II CCD (**2c**) and on a Bruker-AXS, D8 QUEST ECO, PHOTON II area detector (**2c**' and **2e**) diffractometers, using monochromatic radiation $\lambda$(Mo $K_\alpha$) = 0.71073 Å, by means of ω and ϕ scans with a width of 0.50 degree. The data were reduced (SAINT[50]) and corrected for absorption effects by the multi-scan method (SADABS).[51] The structures were solved by direct methods (SIR-2002[52]) and refined against all $F^2$ data by full-matrix least-squares techniques (SHELXTL-2018/3[53]) minimizing $w[F_o^2-F_c^2]^2$. All non-hydrogen atoms were refined anisotropically. The hydrogen atoms were included from calculated positions and refined riding on their respective carbon atoms with isotropic displacement parameters. CCDC 1991478 (**2c**), 2114428 (**2c'**) and 2114429 (**2e**) contain the supplementary crystallographic data for this paper. The data can be obtained free of charge *via:* https://www.ccdc.cam.ac.uk/structures/.

**Computational details.** The electronic structure and geometries of transition states and intermediates of the H-D exchange mechanism were investigated by using density functional theory at the B3LYP level[54,55] with the 6-311++G** basis set. Frequency calculations were carried out at the same level of theory to identify all stationary points as transition states (one imaginary frequency) or as minima (zero imaginary frequencies) and to provide the thermal correction to free energies at 298.15 K and 1 atm. Molecular geometries were optimised without symmetry restrictions. Coordinates of optimised compounds are reported in Table S4. The DFT calculations were performed using the Gaussian 09 suite of programs.[56]

**Antimicrobial studies and microbiological assays**

**Bacterial strains and culture conditions.** As Gram-positive bacteria two staphylococcal species were used: *Staphylococcus pseudintermedius* LMG 22219 was retrieved from the Belgium Coordinate Collection of Microorganisms, whereas *Sthapylococcus aureus* CECT 5190 was retrieved from the Spanish Culture Collection (University of Valencia). On the other hand, as Gram-negative species both *Escherichia coli* CECT 434 and *Pseudomonas aeruginosa* CECT 110 were retrieved from the Spanish Culture Collection. All the strains were streaked out on plates of tryptone soy agar (TSA) to obtain individual colonies. For conservation, liquid cultures were prepared in tryptone soy broth (TSB). Glycerol was added to aliquots of the cultures up to 15% (v:v) and the cultures were stored frozen at -76 °C. All microbiological experiments were performed in aerobiosis and absence of light.

**Determination of minimal inhibitory growth concentrations (MIC) and minimal bactericidal concentrations (MBC).** For the realization of quantitative test to determine the MIC, stock solutions of complexes **2** were prepared at a concentration of 10 mg·mL$^{-1}$. The MIC was performed in 96-well microtiter plates. Serial dilutions (base two logarithmic dilutions from 1024 to 1 mg·L$^{-1}$) of **2** were prepared in Müeller-Hinton broth. Two hundred microliters of each solution were placed in the wells (in triplicate for each concentration) together with a control well with Müeller-Hinton broth as control of non-inoculated wells. The previous day, cultures of *S. pseudintermedius* or *S. aureus* as well as *E. coli* and *P. aeruginosa* were grown overnight at 37°C and 200 rpm in tryptone soy broth (TSB). The initial optical density of the cultures at 600 nm was determined and adjusted to 1.0 with sterile TSB. The wells of the microtiter plates were inoculated with 5 µL of the cultures of each of the strains, keeping a control row without inoculation. The plates were sealed and incubated at 37°C for 24 h. The MIC for each bacterium towards both compounds was determined after visual observation of turbidity and also by measuring the optical density at 600 nm in a microtiter plate reader ASYS UVM340.[57]

The MBC was determined after spreading 100 µL of the wells in the absence of turbidity on tryptone soy agar (TSA) plates. After that, they were incubated for 24 h at 37°C. The concentration of the wells whose corresponding plates did not show colonies growth was considered as the MBC.[57]

A comparative study between bacterial sensitivity ranges towards $AgNO_3$, considered as the compound of reference for its antimicrobial properties, and the dicarboxylate silver compounds was performed using the determination of MIC and MBC techniques described above for **2**.

DOI: 10.1039/D1DT04217K


To determine whether the ligands **1**, used in the synthesis of compounds **2**, had antimicrobial activity *per se,* MIC assays were also performed.

**Determination of antioxidant enzymes and thiobarbituric acid reactive substances (TBARs).** Bacterial strains were cultivated in 50 mL of TSB medium for 24 h at 37 °C and 200 rpm. The cultures were separated in five aliquots of 10 mL each, the first one was maintained in TSB and the other four were supplemented with silver **2** compounds at 1x MIC and 1x MBC for each strain respectively and were cultivated for additional 24 h at 37°C and 200 rpm. After that, the cultures were centrifuged at 8000 rpm for 5 min., the supernatants were discarded and the bacterial pellets were resuspended in 2.5 mL of extraction buffer (50 mM potassium phosphate, pH 7.0 containing 2 mM EDTA). The bacterial suspensions were sonicated for 3 periods of 30 s (separated by periods of 1 min between bursts to cold the crude extract) using a sonicator Ultrasonic Processor (Hielscher) with amplitude 100% and cycle 0.8. All the procedure was performed in an ice bath. After that, the homogenates were centrifuged at 10,000 g for 10 min at 4°C and the supernatants were transferred to clean tubes to be used for enzyme determinations. All the enzymatic assays were performed at room temperature. Catalase (CAT) activity was measured by following the disappearance of $H_2O_2$ at 240 nm ($\varepsilon$ = 39.4 $mM^{-1}\cdot cm^{-1}$) using a Perkin Elmer Lambda 25 UV/Vis spectrophotometer (Shelton, Connecticut, USA).[58] The reaction mixture was performed in a quartz cuvette containing 800 µL of 50 mM sodium phosphate buffer (pH 7.6), 0.1 mM EDTA and 100 µL of 3% $H_2O_2$. The reaction started with the addition of 100 µL of crude extract and the decrease of the OD at 240 nm was registered for 2 min.

The activity of total peroxidases was analysed by following the oxidation of pyrogallol to purpurogallin by $H_2O_2$ at 420 nm.[59] The reaction was performed in 3 mL spectrophotometer cuvettes and contained in a final volume of 2 ml: 1.5 mL of 10 mM potassium phosphate buffer pH 6.0; 0.1 mL of freshly made 0.4M pyrogallol and 0.1-0.2 mL enzyme extract. The reaction was started by addition of 0.15 mL of freshly made 0.3% (v/v) $H_2O_2$. The mix was incubated at room temperature for 5 min and the absorbance at 420 nm was measured. For the calculation of the activity, a control without enzyme extract was prepared and the basal oxidation of pyrogallol was followed by 5 min. The increase of absorbance due to basal oxidation of pyrogallol was detracted from the increase of absorbance of the samples. The activity was calculated using a molar extinction coefficient of $\varepsilon$ = 12 $mM^{-1}$ $cm^{-1}$.

Additionally, superoxide dismutase (SOD) activity was evaluated spectrophotometrically at 560 nm using the assay based on the photoreduction of nitroblue tetrazolium (NBT) in the presence of riboflavine.[60] A stock solution of 30 mL was prepared containing: 27.5 mL potassium phosphate buffer (pH 7.6), 1 mL of 0.2 M EDTA, 1 mL of freshly prepared 1.5 mM NBT and 0.5 mL Triton X-100. The reaction cuvettes contained, in a total of 3 mL volume, 2.88 mL of stock solution and 20 µL of crude extract. The blank reaction was prepared without crude extract in order to follow the basal photoreduction of NBT. The reaction was started by addition of 0.1 mL of 0.12 mM riboflavin. The cuvettes were exposed to white light (commercial fluorescent lights) for 5 min. After this period, the absorbance at 560 nm was determined. One unit of SOD activity was considered as the amount of enzyme able to inhibit 50% of NBT photoreduction by riboflavin.[60]

For the determination of thiobarbituric acid reactive substances (TBARS) such as malondialdehyde (MDA), bacterial strains were cultivated as described before in the presence of 1 x MIC or 1 x MBC for each strain. Cultures were centrifuged at 8000 rpm for 5 min and pellets were homogenized in 3 mL of 20% trichloroacetic acid, containing 0.5% thiobarbituric acid.[61] The homogenate was extracted at 95°C for 30 min followed by rapid chilling on ice and centrifuged at 8000 g for 5 min. The concentration of TBARS was calculated from the value of the absorbance at 532 nm measured with a PerkinElmer Lambda 25 UV/Vis spectrophotometer (Shelton, Connecticut, USA), using the molar extinction coefficient $\varepsilon$ = 155 $mM^{-1}\cdot cm^{-1}$. Moreover, protein content of crude extracts was determined using the method of Bradford,[62] according to a calibration curve using bovine serum albumin (fraction V, Sigma) as standard.

**Effects on biofilm formation: evaluation by colorimetric technique and by Scanning Electron Microscopy (SEM).** The effect on biofilm formation by the bacterial strains was evaluated using 96-well microtiter plates. Aliquots of 200 µL TSB medium (controls) or TSB medium supplemented with complexes **2** in a concentration range from 1024 to 1 $mg\cdot L^{-1}$ were added in triplicate to the wells of the plate. After that, the wells were inoculated with 5 µL of overnight cultures of the bacterial cultures, whose optical density at 600 nm was previously determined and adjusted to 1.0 with sterile TSB. Control rows containing increasing concentration of either of the products were kept without inoculation. The microtiter plate was sealed and incubated at 28 °C for 24 h. For biofilm staining after incubation, the plate was emptied, and the wells were washed thrice with 200 µL of distilled water. Then, the plate was allowed to dry at room temperature and 200 µL of crystal violet (1% w:v) were added to each well and staining was performed for 15 min. After washing the plate three times with water, 200 µL of a solution of acetic acid:ethanol (33%:67% v:v) were added to each well and the plate was incubated at room temperature for 30 min. Finally, the absorbance at 570 nm was measured in comparison to those of wells containing the corresponding media without bacteria.[49]

The formation of biofilms onto a glass surface was evaluated by SEM. Circular glass slides of 1 cm diameter were placed at the fund of the wells of 24-wells polystyrene plates. Aliquots of 2 mL of TSB medium (controls) or TSB medium supplemented with silver **2** compounds at 1 x MIC and 1 x MBC for each bacterium were added to the bottom of the wells (sufficient volume to cover the glass slide). Then, the wells were inoculated with 100 µL of overnight grown cultures of each bacterial strain (optical density adjusted to 1.0). The plates were sealed and incubated at 28 °C for 4 days to allow the biofilm formation. After this time, the glass slides were carefully replaced to a clean plate, washed three times with sterile distilled water and allowed to dry at room temperature. Bacteria on the slides were fixed with 5 mL 2.5 % glutaraldehyde prepared in 0.2 M cacodilate buffer pH 7.2 for 3 h at room temperature. After washing three times with 5 mL 0.2 M cacodilate buffer pH 7.2, samples were dehydrated in acetone series (50% to 100%) and dried using a critical point drier Leica EM CPD300 at 31°C and 73.8 bar. Dried samples were sputtered with Au-Pd (10 nm) and observed with a scanning electron microscope Zeiss EVO LS15.

## Conclusions

Complexes [Ag($L^R$)], **2** ($L^R$ = 2,2'-(imidazolium-1,3-diyl)di(2-*alkyl*acetate)), were obtained by reaction between $Ag_2O$ and $HL^R$, **1**, compounds. They were structurally characterised as homochiral 1D ({Ag[(*S,S*)-$L^{iPr}$]}$_n$, **2c**, and {Ag[(*R,R*)-$L^{iPr}$]}$_n$, **2c'**) or 2D ({Ag[(*S,S*)-$L^{sBu}$]}$_n$, **2e**) coordination polymers, in which the silver cation acts as a bridging linker displaying novel coordination modes. The antimicrobial behaviour of these silver complexes was investigated *versus* Gram-negative bacteria *E. coli* and *P. aeruginosa*. In general, the antimicrobial activity of these compounds is similar to related silver carboxylate derivatives and, in some cases, greater than that of the well-known anti-bactericidal $AgNO_3$, suggesting the major contribution of the coordinated ligand to this effect. From the observed MIC and MBC values, complexes **2b'** and **2c'** showed slightly better antimicrobial properties than those of their enantiomeric derivatives **2b** and **2c**. This fact reveals a possible chirality-antimicrobial tendency. In particular, **2b'** had a wider applicability as an antimicrobial agent than **2c'** and the behaviour of the latter as a eutomer was confirmed by the effect on the biofilm formation, both by colorimetric method and by SEM. These results indicate that **2a** and **2b'** had interesting properties to be considered as effective antimicrobial agents and alternative to classical drugs. Further studies are in progress in order to analyse the action mechanism of these complexes and to evaluate the activity of chemically related silver complexes.

## Conflicts of interest

There are no conflicts to declare.

## Acknowledgements

Financial support from the Ministerio de Ciencia, Innovación y Universidades (PGC2018-093443-B-I00 and PID2019-109371GB-I00) and Junta de Andalucía (US-1380878) is gratefully acknowledged. C. J. C. thanks a research contract from PAIDI 2020, supported by the European Social Fund and Junta de Andalucía. We thank to the Centro de Servicios de Informática y Redes de Comunicaciones (CSIRC), Universidad de Granada, for providing the computing time.

## Author Contributions

Conceptualization, F.M. and A.A.; methodology, F.M. and A.A.; investigation, C.J.C. and M.P.-A.; resources, F.M., A.G., E.A. and E.P.; writing—original draft, F.M.; writing—review and editing, A.A., A.G.; funding acquisition, A.G., A.A. E.P. All authors have read and agreed to the published version of the manuscript.

## Notes and references

1 O. Kühl, S. Millinghaus and P. Wehage, *Open Chem.*, 2010, **8**, 1223–1226.
2 O. Kühl and G. Palm, *Tetrahedron: Asymmetry*, 2010, **21**, 393–397.
3 D. Esposito, S. Kirchhecker and M. Antonietti, *Chem. - A Eur. J.*, 2013, **19**, 15097–15100.
4 S. Kirchhecker, M. Antonietti and D. Esposito, *Green Chem.*, 2014, **16**, 3705–3709.
5 A. Ferry, K. Schaepe, P. Tegeder, C. Richter, K. M. Chepiga, B. J. Ravoo and F. Glorius, *ACS Catal.*, 2015, **5**, 5414–5420.
6 M. A. Reynoso-Esparza, I. I. Rangel-Salas, A. A. Peregrina-Lucano, J. G. Alvarado-Rodríguez, F. A. López-Dellamary-Toral, R. Manríquez-González, M. L. Espinosa-Macías and S. A. Cortes-Llamas, *Polyhedron*, 2014, **81**, 564–571.
7 D. A. Lomelí-Rosales, I. I. Rangel-Salas, A. Zamudio-Ojeda, G. G. Carbajal-Arízaga, C. Godoy-Alcántar, R. Manríquez-González, J. G. Alvarado-Rodríguez, D. Martínez-Otero and S. A. Cortes-Llamas, *ACS Omega*, 2016, **1**, 876–885.
8 E. Steeples, A. Kelling, U. Schilde and D. Esposito, *New J. Chem.*, 2016, **40**, 4922–4930.
9 X. Wang, X. B. Li, R. H. Yan, Y. Q. Wang and E. Q. Gao, *Dalton Trans.*, 2013, **42**, 10000–10010.
10 C. N. Babu, A. Sathyanarayana, S. M. Mobin and G. Prabusankar, *Inorg. Chem. Commun.*, 2013, **37**, 222–224.
11 A. I. Nicasio, F. Montilla, E. Álvarez, R. P. Colodrero and A. Galindo, *Dalton Trans.*, 2017, **46**, 471–482.
12 C. J. Carrasco, F. Montilla and A. Galindo, *Catal. Commun.*, 2016, **84**, 134–136.
13 C. Carrasco, F. Montilla and A. Galindo, *Molecules*, 2018, **23**, 1595.
14 P. Caballero, R. M. P. Colodrero, M. del M. Conejo, A. Pastor, E. Álvarez, F. Montilla, C. J. Carrasco, A. I. Nicasio and A. Galindo, *Inorg. Chim. Acta*, 2020, **513**, 119923.
15 R. Somayaji, M. A. R. Priyantha, J. E. Rubin and D. Church, *Diagn. Microbiol. Infect. Dis.*, 2016, **85**, 471–476.
16 E. Christaki, M. Marcou and A. Tofarides, *J. Mol. Evol.*, 2020, **88**, 26–40.
17 C. Boireau, É. Morignat, G. Cazeau, N. Jarrige, É. Jouy, M. Haenni, J.-Y. Madec, A. Leblond and É. Gay, *Zoonoses Public Health*, 2018, **65**, e86–e94.
18 C. L. Cain, *Vet. Clin. North Am. Small Anim. Pract.*, 2013, **43**, 19–40.
19 P. Fungwithaya, P. Chanchaithong, N. Phumthanakorn and

N. Prapasarakul, *Can. Vet. J.*, 2017, **58**, 73–77.
20 E. I. Vingopoulou, G. A. Delis, G. C. Batzias, F. Kaltsogianni, A. Koutinas, I. Kristo, S. Pournaras, M. N. Saridomichelakis and V. I. Siarkou, *Vet. Microbiol.*, 2018, **213**, 102–107.
21 L. Thornton, V. Dixit, L. O. N. Assad, T. P. Ribeiro, D. D. Queiroz, A. Kellett, A. Casey, J. Colleran, M. D. Pereira, G. Rochford, M. McCann, D. O'Shea, R. Dempsey, S. McClean, A. F. A. Kia, M. Walsh, B. Creaven, O. Howe and M. Devereux, *J. Inorg. Biochem.*, 2016, **159**, 120–132.
22 K. Nomiya, S. Takahashi, R. Noguchi, S. Nemoto, T. Takayama and M. Oda, *Inorg. Chem.*, 2000, **39**, 3301–3311.
23 N. C. Kasuga, Y. Takagi, S. Tsuruta, W. Kuwana, R. Yoshikawa and K. Nomiya, *Inorganica Chim. Acta*, 2011, **368**, 44–48.
24 A. Takayama, Y. Takagi, K. Yanagita, C. Inoue, R. Yoshikawa, N. C. Kasuga and K. Nomiya, *Polyhedron*, 2014, **80**, 151–156.
25 A. Takayama, R. Yoshikawa, S. Iyoku, N. C. Kasuga and K. Nomiya, *Polyhedron*, 2013, **52**, 844–847.
26 K. Nomiya, S. Takahashi and R. Noguchi, *J. Chem. Soc. Dalton Trans.*, 2000, 1343–1348.
27 K. Nomiya, S. Takahashi and R. Noguchi, *J. Chem. Soc. Dalton Trans.*, 2000, **12**, 4369–4373.
28 N. C. Kasuga, A. Sugie and K. Nomiya, *Dalton Trans.*, 2004, 3732–3740.
29 N. C. Kasuga, R. Yoshikawa, Y. Sakai and K. Nomiya, *Inorg. Chem.*, 2012, **51**, 1640–1647.
30 S. Patil, A. Deally, B. Gleeson, H. Müller-Bunz, F. Paradisi and M. Tacke, *Metallomics*, 2011, **3**, 74–88.
31 K. M. Hindi, T. J. Siciliano, S. Durmus, M. J. Panzner, D. A. Medvetz, D. V. Reddy, L. A. Hogue, C. E. Hovis, J. K. Hilliard, R. J. Mallet, C. A. Tessier, C. L. Cannon and W. J. Youngs, *J. Med. Chem.*, 2008, **51**, 1577–1583.
32 A. Kascatan-Nebioglu, M. J. Panzner, C. A. Tessier, C. L. Cannon and W. J. Youngs, *Coord. Chem. Rev.*, 2007, **251**, 884–895.
33 S. Patil, A. Deally, B. Gleeson, F. Hackenberg, H. Müller-Bunz, F. Paradisi and M. Tacke, *Z Anorg Allg Chem.*, 2011, **637**, 386–396.
34 A. Kascatan-Nebioglu, A. Melaiye, K. Hindi, S. Durmus, M. J. Panzner, L. A. Hogue, R. J. Mallett, C. E. Hovis, M. Coughenour, S. D. Crosby, A. Milsted, D. L. Ely, C. A. Tessier, C. L. Cannon and W. J. Youngs, *J. Med. Chem.*, 2006, **49**, 6811–6818.
35 S. Roland, C. Jolivalt, T. Cresteil, L. Eloy, P. Bouhours, A. Hequet, V. Mansuy, C. Vanucci and J.-M. Paris, *Chem. - A Eur. J.*, 2011, **17**, 1442–1446.
36 Y. Sarı, S. Akkoç, Y. Gök, V. Sifniotis, İ. Özdemir, S. Günal and V. Kayser, *J. Enzyme Inhib. Med. Chem.*, 2016, **31**, 1527–1530.
37 R. Sakamoto, S. Morozumi, Y. Yanagawa, M. Toyama, A. Takayama, N. C. Kasuga and K. Nomiya, *J. Inorg. Biochem.*, 2016, **163**, 110–117.
38 M. Pellei, V. Gandin, M. Marinelli, C. Marzano, M. Yousufuddin, H. V. R. Dias and C. Santini, *Inorg. Chem.*, 2012, **51**, 9873–9882.
39 J. Guo, Y. Qian, B. Sun, Z. Sun, Z. Chen, H. Mao, B. Wang and F. Yan, *ACS Appl. Bio Mater.*, 2019, **2**, 4418–4426.
40 D. Lopez, H. Vlamakis and R. Kolter, *Biofilms. Cold Spring Harb. Perspect. Biol.*, 2010, **2**, a000398–a000398.
41 I. Alkorta, J. Elguero and A. Frontera, *Crystals*, 2020, **10**, 180.
42 Z. Fei, W. H. Ang, T. J. Geldbach, R. Scopelliti and P. J. Dyson, *Chem. - A Eur. J.*, 2006, **12**, 4014–4020.
43 C. R. Groom, I. J. Bruno, M. P. Lightfoot and S. C. Ward, *Acta Crystallogr. Sect. B Struct. Sci. Cryst. Eng. Mater.*, 2016, **72**, 171–179.
44 C. J. Carrasco, F. Montilla, E. Alvarez, A. Galindo, M. Perez-Aranda, E. Pajuelo and A. Alcudia, *Manuscrip submitted for publication.*
45 R. B. Thurman and C. P. Gerba, *Crit. Rev. Environ. Control*, 1989, **18**, 295–315.
46 K. Nomiya, K. Tsuda, T. Sudoh and M. Oda, *J. Inorg. Biochem.*, 1997, **68**, 39–44.
47 K. Asaad and S. Mashhadi, *Int. J. Low. Extrem. Wounds*, 2013, **12**, 324–324.
48 D. Cherian, T. Peter, A. Narayanan, S. Madhavan, S. Achammada and G. Vynat, *J. Pharm. Bioallied Sci.*, 2019, **11**, 297–300.
49 G. A. O'Toole, *J. Vis. Exp.*, 2011, e2437.
50 Bruker, *SAINT+*, 2007, Bruker AXS Inc., Madison, Wisconsin, USA.
51 G. M. Sheldrick, *SADABS, Programs Scaling Absorpt. Correct. Area Detect. Data*, 1997, University of Göttingen: Göttingen, Germany.
52 M. C. Burla, M. Camalli, B. Carrozzini, G. L. Cascarano, C. Giacovazzo, G. Polidori and R. Spagna, *J. Appl. Crystallogr.*, 2003, **36**, 1103–1103.
53 G. M. Sheldrick, *Acta Crystallogr. Sect. A Found. Crystallogr.*, 2008, 64, 112–122.
54 A. D. Becke, *J. Chem. Phys.*, 1993, **98**, 5648–5652.
55 C. Lee, W. Yang and R. G. Parr, *Phys. Rev. B*, 1988, **37**, 785–789.
56 C. G. and J. A. P. M. J. Frisch, G. W. Trucks, H. B. Schlegel, G. E. Scuseria, M. A. Robb, J. R. Cheeseman, J. A. Montgomery Jr., T. Vreven, K. N. Kudin, J. C. Burant, J.M.Millam, S. S. Iyengar, J. Tomasi, V. Barone, B. Mennucci, M. Cossi, G. Scalmani, N. Rega, G. A. Peters, *Gaussian, Inc., Wallingford CT*, 2009.
57 S. J. Cavalier, R. J. Harbeck, Y. S. McCarter, J. H. Ortez, I. D. Rankin, R. L. Sautter, S. E. Sharp and C. A. Spiegel, *Man. Antimicrob. susceptibility Test.*, 2005, **32**, 53–62.
58 L. Pine, P. S. Hoffman, G. B. Malcolm, R. F. Benson and M. G. Keen, *J. Clin. Microbiol.*, 1984, **20**, 421–9.
59 B. Chance and A. C. Maehly, *Methods Enzymol.*, 1955, **2(C)**, 764–775.
60 W. F. Beyer and I. Fridovich, *Anal. Biochem.*, 1987, **161**, 559–566.
61 K. S. Ong, Y. L. Cheow and S. M. Lee, *J. Adv. Res.*, 2017, **8**, 393–398.
62 M. M. Bradford, *Anal. Biochem.*, 1976, **72**, 248–54.